Applied Thermal Engineering 215 (2022) 118945

Contents lists available at ScienceDirect

Applied Thermal Engineering

journal homepage: www.elsevier.com/locate/apthermeng

Research Paper

Improving magnetic cooling efficiency and pulldown by varying flow profiles

M. Masche, J. Liang, K. Engelbrecht *, C.R.H. Bahl

Department of Energy Conversion and Storage, Technical University of Denmark (DTU), Anker Engelunds Vej B301, 2800 Kgs. Lyngby, Denmark

ARTICLE INFO

Keywords:
Active magnetic regenerator
Hydraulic circuit
Gadolinium
Flow resistance
Blow fraction

ABSTRACT

Magnetic refrigeration systems are promising cooling solutions that employ the active magnetic regenerator refrigeration cycle to achieve practical temperature spans and environmental benefits. The hydraulic system that ensures a continuous flow of the heat transfer fluid through the system with a reciprocating flow in each regenerator bed is critical to the performance of the refrigeration cycle. Hence, we investigate the characteristics of the parallel flow circuit of a rotary active magnetic regenerator system, which consists of thirteen trapezoid-shaped regenerators, each filled with 295 g of gadolinium spheres. Fluid flow is controlled via electrically actuated solenoid valves (both piloted and direct-acting) connected to the regenerator hot side. By varying the percentage of opening of the control valves, different blow fractions (or fluid flow waveforms) could be investigated. The objective of the study is twofold: (i) assess whether flow imbalances of the heat transfer fluid exist in the cold-to-hot blow (cold blow) and hot-to-cold blow (hot blow) directions, and (ii) determine whether there is an optimal value of the blow fraction both to maximize the cooling performance and realize a rapid temperature pulldown. Flow resistance measurements demonstrate a symmetric flow circuit design and resistances that are similar in the cold and hot blow directions. Moreover, for the studied temperature spans of 6 K and 16 K, the best blow fraction was found to be about 41.6 %. For instance, at a 16 K span, a utilization of 0.32, and at 1.4 Hz, increasing the fluid blow fraction from 25.0 to 41.6 % enhanced the cooling capacity and second-law efficiency from 70 to 330 W and from 2.6 to 17.4 %, respectively. In turn, lower blow fractions favored a more rapid temperature pulldown. The magnetocaloric system was about 30 % faster in establishing approximately 14 K temperature span when the blow fraction was reduced from 41.6 to 30.6 %. Hence, magnetic refrigeration systems can benefit greatly from solenoid valves, which allow the system to operate either in a time-saving mode or an energy-saving mode.

1. Introduction

Magnetic refrigeration, which makes use of Active Magnetic Regenerators (AMRs), is a viable alternative to traditional vapor compression systems [1]. AMRs exploit the MagnetoCaloric Effect (MCE), which is observed as a reversible temperature change when a solid-state MagnetoCaloric Material (MCM) is magnetized or demagnetized. The magnetization of the MCM is analogous to compressing a gaseous refrigerant (heating), while the demagnetization is analogous to expanding a gas (cooling). Consequently, magnetocaloric appliances can replace the traditional vapor compression-expansion cycle and avoid the problems that come with it, such as the use of global warming potential refrigerants [2]. Magnetic refrigeration also eliminates the need for compressors with moving parts, resulting in less mechanical vibration and noise. Moreover, magnetic refrigeration may attain higher second-law efficiencies than traditional refrigerators [3], making it a more efficient cooling technology.

AMR systems consist of the MCM that undergoes the active magnetic regenerator cycle, which is made up of two main processes: magnetization and demagnetization. During magnetization, excess heat generated by the MCE can be rejected to a hot reservoir, and a cooling load can be accepted from a cold reservoir during demagnetization. To transport energy between the external heat exchangers and the AMR beds, a water-based heat transfer fluid is continually pumped either through a single-layered or multi-layered regenerator bed [4–10] or a configuration of multiple beds [11–26] synchronized with the changing applied magnetic field. In rotary multi-bed AMR devices, the magnetic field generated by the magnet can be utilized continuously, which is important because the magnet is the most costly component in an AMR system

* Corresponding author.
E-mail address: kuen@dtu.dk (K. Engelbrecht).

https://doi.org/10.1016/j.applthermaleng.2022.118945
Received 21 February 2022; Received in revised form 3 June 2022; Accepted 2 July 2022
Available online 13 July 2022

Nomenclature

Acronyms

AMR	Active Magnetic Regenerator
BFD	Blow Fraction Differences
HPV	High-Pressure Valve

Roman symbols

B	Magnetic flux density [T]
c	Specific heat capacity [J•kg^{-1}•K^{-1}]
COP	Coefficient of Performance
d	Diameter [μm]
f	Operating (motor) frequency [Hz]
F	Fraction [%]
Gd	Gadolinium
m	Mass [kg]
NTU	Number of transfer unit [-]
p	Pressure [bar]
$\dot{Q}_c$	Cooling power [W]

Greek symbols

Δp	Pressure drop [bar]
Δs	Entropy change [J•kg^{-1}•K^{-1}]
ΔT	Temperature span, T_{hot}-T_{cold} [K]
η_{II}	Second-law efficiency [%]

Subscripts

b	Blow
cb	Cold blow
d	Delay
f	Fluid
hb	Hot blow
LPV	Low-Pressure Valve
MCE	Magnetocaloric Effect
MCM	Magnetocaloric Material
T	Temperature [K]
T_{cold}	Cold reservoir temperature [K]
T_{hot}	Hot reservoir temperature [K]
u	Relative uncertainty [%]
U	Utilization factor [-]
$\dot{V}$	Volumetric flow rate [L/h]
$\dot{W}_{losses}$	Iron losses [W]
$\dot{W}_{mag}$	Magnetic power into regenerator [W]
$\dot{W}_{shaft}$	Shaft power [W]
$\dot{W}_{pump}$	Pumping power [W]
P	Density [kg•m^{-3}]
Γ	Shaft torque [Nm]
τ	AMR cycle period [s]
mag	Magnetic
max	Maximum
O	Offset
P	Particle

[27]. According to Griffith et al. [28], AMR performance is not restricted by the dynamics of the MCE or the heat transfer constraints induced by temperature gradients inside the solid refrigerant. Rather, the effects of the magnetic field profile [29,30], the fluid flow profile [28,31–34], and the timing between the magnetic field and fluid flow profiles [29,30,35] on the AMR performance should be explored.

One of the challenges of rotary multi-bed AMR devices is the operation and control of the hydraulic circuit that allows for continuous fluid flow between the AMR beds and the hot and cold reservoirs while enabling a reciprocating flow in each regenerator bed synchronized with the changing magnetic field. To maximize the heat transfer potential and cooling capacity, the MCM should be fully magnetized before the cold blow begins and remain that way during the entire blow [31]. In a rotary AMR configuration, multiple beds can enter or exit the magnetic field in parallel. Similarly, multiple beds may experience flow in each direction between the two fluid reservoirs. It is ideal for the system to have a balanced flow rate at a constant pressure drop throughout the AMR cycle, analogous to reducing torque fluctuations by magnetically balancing the regenerators [14]. The flow control system has been shown to cause performance reductions due to imbalances in the heat transfer fluid [36–39], friction heat generated in the flow distribution system [26], void volume and uneven inlet flow distribution [40], and balancing the fluid flow through the regenerator beds can improve the AMR performance [39].

In a recent study, Dall'Olio et al. [21] present the design of a rotary thirteen-bed AMR system, named MagQueen, with a parallel hydraulic circuit utilizing a total of 26 electrically operated solenoid valves connected to the in-and outlet of the regenerator hot side. Other flow distribution systems commonly employed in magnetic refrigerators include mechanically actuated valves, such as poppet valves [14] and rotary valves [7,13,22,33,41]. In MagQueen, the percentage of the valve opening, i.e., the blow fraction, can be regulated to correct flow imbalances in each bed and distribute the fluid flow through all beds as desired. Experiments on the MagQueen demonstrated that flow imbalances between beds cause cold side outlet temperature variations and a reduced AMR performance. Individual bed blow fraction adjustments can be used to correct flow imbalances [42]. Active valve management has been shown to enhance the cooling power and Coefficient of Performance (*COP*) by as much as 70 % [43]. Flow imbalances caused by variations in the flow resistance through the beds are partially explained by manufacturing tolerances [36].

According to recent research [32–34,36,39], there are optimal values for the blow fraction that maximize both the cooling capacity and temperature span. A blow fraction that is too low results in a volume flow rate is too high for a fixed utilization, reducing the number of transfer units (*NTU*s) and the regenerator thermal effectiveness, and therefore, the AMR performance [34]. A blow fraction that is too high results in that the heat transfer fluid flows while the applied magnetic field still changes, reducing the heat transfer potential and hence the AMR performance [31]. There are numerous studies in the literature on the performance assessment of AMR devices, but only a few [44–46] deal with the control of such devices. Certain appliances demand a high *COP* or maximum cooling capacity, while others may require a rapid temperature pulldown (cooling). In some cases, a steady temperature span may be more important.

In this study, we investigate whether the cooling performance and temperature pulldown of a rotary multi-bed AMR system can be controlled by adjusting the blow fractions (i.e., the fluid flow waveform). As a baseline for comparison, we use a 7 kW vapor compression heat pump connected to a ground source. The vapor compression system uses R134a as the working fluid and operates between 285.2 K and 298.2 K. Neglecting the pumping power to the ground source, the vapor compression heat pump operates at a COP of 5.0 for a compressor frequency of 60 Hz [47], which is optimized for efficiency but produces lower cooling power. In particular, the effect of the blow fraction on the temperature pulldown is not well documented in the literature. The impact of different blow fractions on the AMR cooling performance was investigated by changing the percentage of opening of a set of pilot-operated High-Pressure Valves (HPVs) connected to the regenerator hot inlet and a set of direct-acting Low-Pressure Valves (LPVs) connected

to the regenerator hot outlet. Furthermore, the influence of blow fraction differences between the HPVs and LPVs on the AMR performance is addressed. The flow resistance of each regenerator bed in the hot-to-cold and cold-to-hot directions is also measured to determine whether flow imbalances exist due to different fluid masses being displaced during the cold and hot blow.

2. Experimental work

2.1. Active magnetic regenerator apparatus

The rotary magnetocaloric refrigeration system investigated in this study is depicted in Fig. 1. MagQueen is a device comprised of thirteen trapezoid-shaped regenerator beds mounted between a laminated iron ring and a rotating two-pole permanent NdFeB magnet. The magnet is surrounded by an iron yoke and driven by an electric motor. A rotary encoder installed on the rotor shaft records the magnet position, and the torque on the rotor shaft is measured by a torque meter. Because an even bed number would cause stable magnetic equilibrium locations during magnet rotation, the number of beds is odd. This reduces cogging torque that would otherwise result in substantial torque fluctuations and, as a result, an unbalanced magnetic power input [14]. Each regenerator bed contains 295 g of packed spheres (350–710 μm in diameter) of gadolinium (Gd) that undergoes periodic magnetization and demagnetization. The choice of size was dictated by material availability. A smaller sphere diameter and a narrower size range should result in higher performance, although at a higher pressure drop. In a 1 T field, a peak magnetic entropy change (Δs_{mag}) of the Gd spheres of 3.5 J $kg^{-1}K^{-1}$ was measured at a temperature of 290.5 K [23]. The average porosity of the bed is 0.381, calculated as the ratio of pore volume to regenerator (bulk) volume. The magnetic field oscillates between 0 and 1.44 T in the 34 mm air gap. Further details about the design and operation of the device can be found in Ref. [21,42]. The accuracies of all sensors (torque meter, thermocouples, pressure transmitters, flow meters, torque sensor, etc.) used during the experiments are given in Table 1, and the overall uncertainties of system-level parameters are given in Table 2.

The AMR device uses a heat transfer fluid composed of 90 vol% deionized water mixed with 10 vol% mono-ethylene-glycol to prevent corrosion of Gd. The fluid transports the heat generated from magnetizing and demagnetizing the solid MCM to the cold and hot side heat exchangers that represent the cold and hot reservoirs of the system. Fig. 2 illustrates the flow of fluid through a single regenerator bed. The fluid is circulated between the cold and hot heat exchangers using a centrifugal pump with an integrated frequency inverter. The pump is able to provide a low volumetric fluid flow rate of 0.5–10 L min^{-1} using a vortex flow meter and a larger flow rate of 5.7–56.8 L min^{-1} using a liquid flow transmitter. The reciprocating flow through each AMR bed is controlled by solenoid valves mounted on the regenerator hot side, and it is synchronized with the changing magnetic field. The opening and closing of the solenoid valves is based on an angle reading from the angular encoder mounted on the rotating magnet. The thirteen hot inlet solenoid valves are pilot-operated high-pressure valves (HPVs) used to control the blow fraction in the hot-to-cold direction. Pilot-operated valves use a diaphragm to seal over a high differential pressure. As the HPVs are mounted at the pump outlet, they experience the highest differential fluid pressure, which assists in performing the main work of opening and closing the valves. The thirteen hot outlet solenoid valves, on the other hand, are direct-acting low-pressure valves (LPVs) that regulate the cold blow and return the cold fluid to the hot reservoir. The fluid pressure is low enough that direct-acting valves can be used.

On the regenerator cold side, 26 check valves with a low cracking pressure (below 0.1 bar) ensure a unidirectional flow through an electrical circulation heater that simulates the cooling load and thus the cold reservoir temperature (T_{cold}). Manifolds for collecting and distributing the working fluid ensure a continuous fluid flow through the system. Additionally, flow strainers equipped with filters protect the flow system from particles leaving the AMR bed or other objects carried by the fluid. A chiller on the hot reservoir uses a counter-flow plate heat exchanger to control the hot reservoir temperature (T_{hot}). The difference between the reservoir temperatures defines the reservoir temperature span (ΔT) of the AMR apparatus. Fluid temperatures were continuously measured inside the manifolds using calibrated resistance temperature detectors to calculate the cooling capacity and ΔT. Temperatures of the working fluid were also measured at the regenerator cold outlet ($T_{cold,out}$) and the regenerator hot outlet ($T_{hot,out}$) using calibrated thermocouples to identify flow imbalances in different AMRs during the cold blow and hot blow, respectively. Pressure transducers were used to calculate the flow resistance through each AMR bed and measure the total system fluid pressure drop. The flow rate, encoder angle, and torque were all continuously monitored.

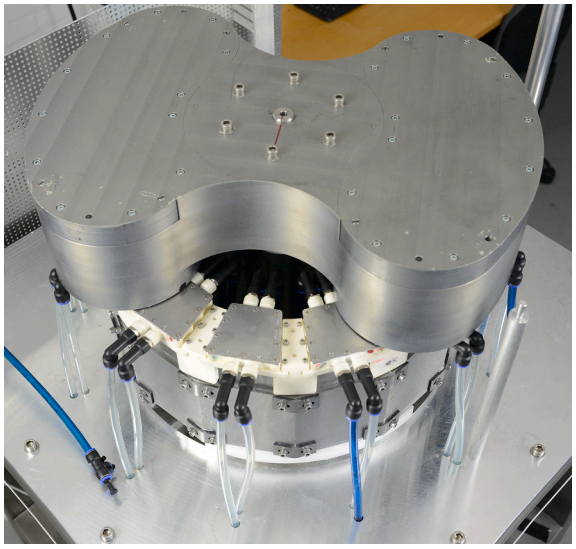

Fig. 1. Top view of the magnetocaloric refrigeration system.

Table 1
Summary of measurements and experimental uncertainties.

Measurement	Characteristics (type)	Accuracy[1]
Temperature	RTD (Pt100)	± (0.15 + 0.002 T) °C
	Thermocouple (E)	± 0.5 K
Torque	Rotary torque sensor	± 1 % of torque
Pressure	Pressure transmitter	± 0.3 % of pressure
Fluid flow rate	High range (5.7–56.8 L/min) flow meter (liquid flow transmitter)	± 2 % of flow
	Low range (0.5–10 L/min) flow meter (vortex)	± 1 % of flow
Cycle frequency	Frequency inverter	± 0.5 % of frequency
Magnet position	Absolut analog encoder	± 0.07 % of angle

Table 2
Estimated relative combined standard uncertainties of calculated values.

	U	R	$\dot{Q}_c$	$\dot{W}_{pump}$	$\dot{W}_{mag}$	ΔT	COP	η_{II}
u [%]	1	2	10	3	2	1	10	10

2.2. Blow fraction control

Different blow fractions (or flow waveforms) are realized by increasing or reducing the opening period of the solenoid valves by an

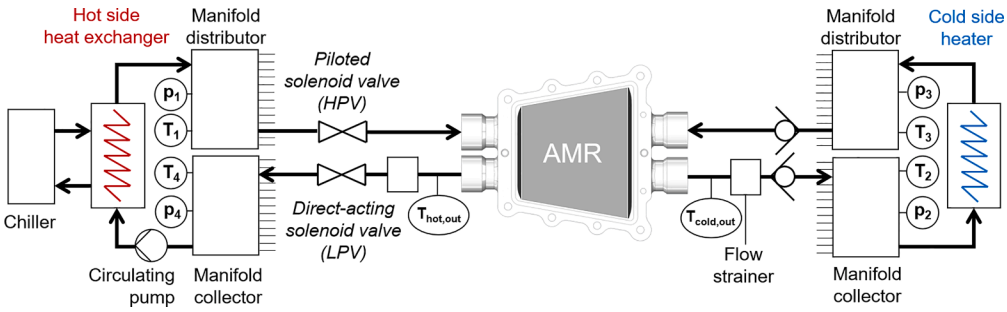

Fig. 2. Simplified sketch of the flow of heat transfer fluid through a single AMR bed and between the external heat exchangers.

electric circuit. The system blow fraction (F_b) is defined as the time fraction of the AMR cycle when fluid is blown through the AMR bed, and it is expressed as follows:

$$F_b = \frac{2\tau_b}{\tau} \tag{1}$$

Where τ_b and τ denote the periods of one fluid blow and the whole AMR cycle, respectively. F_b represents the average value of the cold blow fraction (F_{cb}) and the hot blow fraction (F_{hb}). During the cold blow, the LPVs open and the heat transfer fluid flows from the cold heat exchanger through the AMRs. When the AMR is magnetized, heat is transferred from the solid refrigerant to the fluid during the cold blow. During the hot blow, in turn, the HPVs open and high-temperature fluid re-enters the demagnetized AMRs from the hot heat exchanger. The average blow fractions of 25.0, 30.6, 36.1, 41.6, and 47.2 % were tested in this study. Lower blow fractions indicate that fewer valves open simultaneously and for a shorter period, causing a longer no-flow period (or waiting period) between the blows. At constant utilization, the mass flow rate amplitude per AMR bed increases, as the displaced fluid mass remains constant. All solenoid valves can be controlled separately and while the device is running. Hence, the cold and hot blow fractions for each AMR can be readily adjusted. Moreover, because the AMR inlets are hydraulically connected in parallel, the fluid flow can be distributed in any desired manner based on the valve timing.

Active valve control is not confined to testing only different blow fractions. Also, the timing between when the fluid is blown and when the magnetic field is near its maximum or minimum can be examined. This interplay between magnetic field and fluid flow profiles is known as synchronization [29], and it is a critical control parameter, as a fluid flow profile non-synchronized with the magnetic field profile can degrade the AMR cooling performance [28,29,35]. In this paper, the AMR cycle is synchronized when the two profiles are centered, i.e., there is no delay between the mid-points of the periods of cold/hot blow and magnetization/demagnetization (Fig. 3). Hence, an offset fraction (F_o) can be defined as:

$$F_o = \frac{2\tau_d}{\tau} \tag{2}$$

Where τ_d is the delay time between the midpoints of the periods of cold/hot blow and magnetization/demagnetization. In the AMR device, the delay time, which depends on the encoder angle reading, can be changed by varying the offset fraction of the cold/hot blow period. A positive offset fraction means that the cold/hot blowing period has been shifted, i.e., the blow starts later than in the centered profile alignment in the AMR cycle.

Fig. 3 shows the magnetic flux density and the fluid flow profiles, as well as the symbols used in Eq. (1) and Eq. (2). As depicted, 1 AMR cycle has two identical fluid blows in each direction. In general, the flow profile displays when the valves are open, i.e., the fluid is flowing through the bed (i.e., the blow period), and when the valves are closed, i.e., no fluid is flowing through the bed (i.e., the waiting period). It can be seen that the magnetic field waveform is well represented by a step

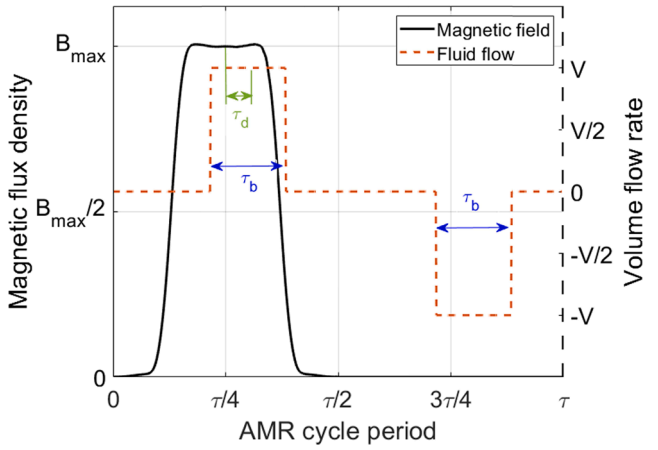

Fig. 3. Magnetic flux density profile (solid line) and fluid flow profile (dashed line) of the AMR cycle showing the fluid blow period (τ_b) and delay time (τ_d) between the mid-points of the periods of cold blow and magnetization.

change, i.e., the changes in the magnetic flux density between the maximum and minimum value occur with a fast ramp time and nearly instantaneously, which is close to the waveform of the idealized Brayton cycle. The ability to perform the AMR cycle with a step change for the magnetic flux density provides the highest cooling capacity and regenerator temperature span compared to field waveforms that change continuously throughout the cycle, such as sinusoidal or rectified sinusoidal waveforms [48]. The flow profile is the same in all thirteen beds. It is worth noting that discussing various flow profiles in relation to the magnetic field may result in changing working regimes and hence performing different thermodynamic cycles [30]. In the AMR design with thirteen beds and a two-pole permanent magnet, six/seven beds are always open in parallel during the cold blow, while seven/six beds are always open in parallel during the hot blow. This means that during the AMR cycle, fluid is always flowing through each bed, and the no-flow period is minimal.

2.3. Performance metrics and experimental conditions

The impact of the fluid flow characteristics on the performance of the rotary AMR device was assessed over a wide range of operating conditions. The timing between magnetic field profile and fluid flow profile (i.e., the AMR cycle timing), the fluid blow fraction, and the Blow Fraction Differences (BFD) between the HPVs and LPVs have all been investigated. Experiments were run at different utilization factors and two reservoir temperature spans. Two spans of about 6 K and 16 K were achieved by maintaining the hot reservoir temperature at 301 K and setting the cold reservoir temperature to 295 K and 285 K, respectively. To allow the comparison to other AMR systems, the volumetric flow rate is presented as the utilization factor, which relates the thermal capacity of the working fluid passing through the AMR bed during one blow

(cold/hot blow) to the thermal capacity of the solid refrigerant:

$$U = \frac{\rho_f c_f \dot{V}}{2 f m_s c_s} \tag{3}$$

Where c_s represents the average specific heat capacity of the solid MCM, which is set to $c_s = 380$ J kg^{-1} K^{-1}, as per [49]. The total mass of MCM is $m_s = 3.83$ kg. The fluid properties were estimated using the commercial software Engineering Equation Solver [50] at a reference temperature of 293 K. A low value of U implies that a low amount of fluid flows through the AMR bed. The AMR cooling performance has been shown to be optimum at a specific utilization factor for a given regenerator geometry, frequency, and temperature span [32,33,51].

The flow (or hydraulic) resistance was measured during the cold blow (R_{cb}) and hot blow (R_{hb}) to assess the level of imbalance of the heat transfer fluid between the flow paths in and out of each AMR bed. The relationship between the pressure drop across the AMR bed and the volume flow rate is described by the flow resistance. Thus, the flow resistance can be defined as:

$$R = \frac{\Delta p}{\dot{V}} \tag{4}$$

As shown in Fig. 2, the pressure drop during the cold blow and hot blow is defined as $\Delta p_{cb} = p_3$-p_4 and $\Delta p_{hb} = p_1$-p_2, respectively. The pressures p_1, p_2, and p_3 are measured in the three manifolds, while p_4 represents the atmospheric pressure and is assumed to be zero.

The main input power to drive the AMR cycle comes from the magnetic (or AMR) power ($\dot{W}_{mag}$) delivered to the MCM and the pumping power ($\dot{W}_{pump}$) required to overcome the viscous losses, which are a function of the pressure drop across the AMR bed. The latter is given by:

$$\dot{W}_{pump} = \dot{V}(p_1 - p_2 + p_3 - p_4) \tag{5}$$

Due to the fact that the pump is not optimized for a particular operating condition, only the shaft work is considered here and not the plug power to the pump. The power consumption of the solenoid valves is excluded from the input power. $\dot{W}_{mag}$ is calculated by subtracting the power losses ($\dot{W}_{losses}$), which are a function of the AMR frequency (f_{AMR}), from the shaft power ($\dot{W}_{shaft}$) needed to rotate the magnetic circuit. As demonstrated in [43], $\dot{W}_{losses}$ comprises power losses caused by eddy currents induced in the laminated iron ring and frictional losses in the bearings and couplings. $\dot{W}_{mag}$ is hence defined as follows:

$$\dot{W}_{mag} = \dot{W}_{shaft} - \dot{W}_{losses} \tag{6}$$

Where $\dot{W}_{shaft}$ is given by.

$$\dot{W}_{shaft} = 2\pi f \Gamma \tag{7}$$

Where f is the operating frequency, which is half of f_{AMR}, because the two-pole permanent magnet generates two high fields. Γ is the torque instantaneously measured at the shaft.

The cooling power ($\dot{Q}_c$) produced by the AMR device is calculated as follows:

$$\dot{Q}_c = \dot{V} \rho_f c_f \Delta T_{cold} \tag{8}$$

This leads to the important calculation of the COP and second-law efficiency (η_{II}), which are given by:

$$COP = \frac{\dot{Q}_c}{\dot{W}_{mag} + \dot{W}_{pump}} \tag{9}$$

And.

$$\eta_{II} = \frac{COP}{COP_{ideal}} \tag{10}$$

Where the ideal COP (COP_{ideal}) is defined as:

$$COP_{ideal} = \frac{T_{cold}}{T_{hot} - T_{cold}} \tag{11}$$

The relative combined standard uncertainties (u) of the calculated values were estimated using the Taylor Series Method (TSM) [52]. For the magnetic power uncertainty, only the system uncertainty was considered, because fluctuations in the power measurements are caused by the AMR internal operation and not from random error sources [53,54]. For each test condition, a sampling frequency of around 6 Hz was used. All performance data presented in this paper were averaged over a 10-min period after reaching steady-state operating conditions. The steady-state operation was achieved when the standard deviation of the measured reservoir temperature span was below 0.05 K for more than 2 min.

3. Results and discussion

3.1. Regenerator flow resistance during cold and hot blow

Fig. 4 shows the measured pressure drop across each mounted bed versus the volume flow rate during the cold and hot blows, respectively. The pressure drop was measured at four volumetric fluid flow rates (100, 160, 275, and 350 L h^{-1}), which correspond to typical flow rates during normal AMR system operation at low frequency. The measurements were performed near room temperature (about 295 K) and without the magnetic circuit rotating. Fig. 4 also depicts the original average pressure drop data during the cold blow for each AMR bed without the solenoid valves, as it was demonstrated in Ref. [43]. As with the original data, the pressure drop across the mounted beds follows a parabolic relationship with the volume flow rate consistent with the Ergun-like equation [55].

In both flow directions, small pressure drop differences between the beds can be noticed. These can be caused by a variety of factors, including manual filling and compression of the MCM, manufacturing tolerances of the bed housing, differences in the external tubing, flow distribution in manifolds, and the wide particle size distribution of Gd spheres in the packed bed. The latter is particularly significant, as wider particle size distributions increase the inhomogeneity and randomness of the packing structure [56], leading to diverse arrangements of differently-sized spheres in the packed bed. The effects of flow channeling on pressure drop differences are believed to be minor, as they result in cold or hot bypassed fluid and a reduced thermal performance

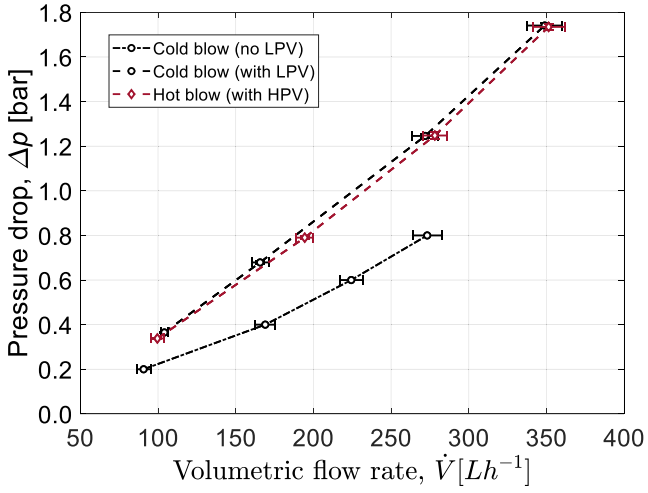

Fig. 4. Average pressure drop measurements during the cold and hot blows through each of the thirteen mounted AMR beds. The error bars indicate the standard deviation of the mean, and they are shown when larger than the data symbol.. For comparison, the original pressure drop measured without solenoid valves during the cold blow is also plotted for each bed as per Ref. [43].

of the regenerator [57]. Care was taken during the regenerator assembly to avoid the formation of void regions at the bed wall by applying pressure on a silicon foam layer placed on top of the material bed. Additionally, pressure drop variations increase with increasing flow rates. Hence, during normal AMR operation at higher flow rates, larger variations of the flow resistance will be more likely.

Despite the high level of complexity of the hydraulic circuit (see Fig. 2), the average pressure drop data in the cold-to-hot and hot-to-cold directions appear to be relatively comparable, implying a symmetric design of the hydraulic circuit and a balanced flow resistance in both directions. Other research has found that discrepancies between the cold and hot fluid blows for AMR devices are not unusual [37–39,58]. Nakashima et al. [37] attributed flow imbalances during the cold and hot blows to torque oscillations of the magnetic circuit that resulted in non-uniform rotation of the rotary valves. Other authors [38,58] found that variations in the solid thermal mass result in different heat transfer rates (and effectiveness) for each blow. The authors ascribed their finding to the temperature dependency of the specific heat capacity of Gd, i.e., its specific heat is greater at lower temperatures than at higher temperatures. In the present study, the cold and hot blows follow nearly the same trend, and there is no asymmetry between the two blow periods. This is because the pressure drop was measured at ambient temperature and without rotating the magnet, resulting in nearly identical temperatures near the regenerator cold and hot ends, and therefore similar solid thermal masses at both ends. However, during normal AMR operation, when a temperature span of up to 16 K is imposed on the regenerator, solid thermal mass variations are to be expected.

The ratio of normalized cold blow flow resistance (R^*_{cb}) to normalized hot blow flow resistance (R^*_{hb}), shown in Fig. 5 addresses the issue regarding the occurrence of differences in the bed flow resistance. The measured flow resistance for an individual bed was normalized by dividing it by the mean value of the thirteen beds. A ratio of one implies equal relative flow resistances in both directions. As can be seen, most beds have nearly equal blow periods within their uncertainty range, suggesting that flow resistance differences between the flow paths in and out the AMR beds are minimal. The flow resistances during the cold and hot blows at various flow rates are, on average, $\overline{R}_{cb} = 0.258(\pm 0.039)\,\mathrm{bar\,min\,L^{-1}}$ and $\overline{R}_{hb} = 0.253(\pm 0.039)\,\mathrm{bar\,min\,L^{-1}}$, respectively. In comparison to the remaining beds, only regenerator 11 appears to be an outlier with a higher flow resistance in the hot-to-cold direction, and thus, the hot blow is executed over a shorter period. To realize a similar flow across each bed, beds with similar flow resistances should be open in one direction. Studies have shown that an unbalanced flow resistance in an AMR causes variations in the temperature of the fluid exiting the regenerator cold end, which is detrimental to the AMR cooling capacity and *COP* [36,43]. As a consequence, a flow balancing procedure, as described in [43], was performed. For example, the higher flow resistance in the hot-to-cold direction in bed 11 can be quantified by a lower regenerator $T_{cold,out}$ in the system. The $T_{cold,out}$ can then be adjusted by balancing the blow fraction of the HPVs connected to the regenerator hot inlet, hence balancing the flow resistance in bed 11. Thus, the results presented in the following sections are based on balanced flow conditions to realize equal flow resistances across each AMR and optimum operating conditions in each AMR.

3.2. Timing between magnetic field and fluid flow

The effect of the timing between magnetic field and fluid flow profiles on the AMR performance has been investigated by varying the delay time between the midpoints of the cold/hot fluid blow and magnetization/demagnetization periods. Fig. 6a presents the performance results. It shows the data for tests run at a cycle frequency of 0.5 Hz, cold and hot blow fractions of 36 %, and a flow rate of about 520 L/h ($U = 0.41$). The

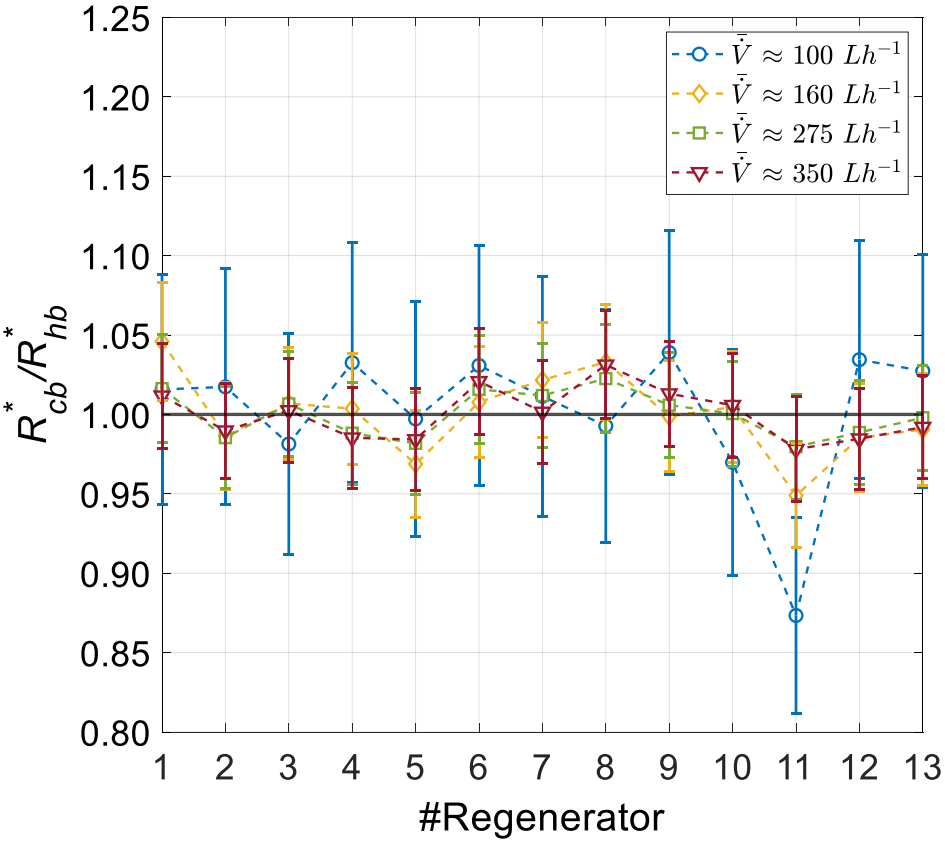

Fig. 5. Ratio of normalized cold-blow flow resistance to normalized hot-blow flow resistance for each AMR bed at different average flow rates. The error bars represent the combined absolute uncertainty associated with the flow resistance measurements.

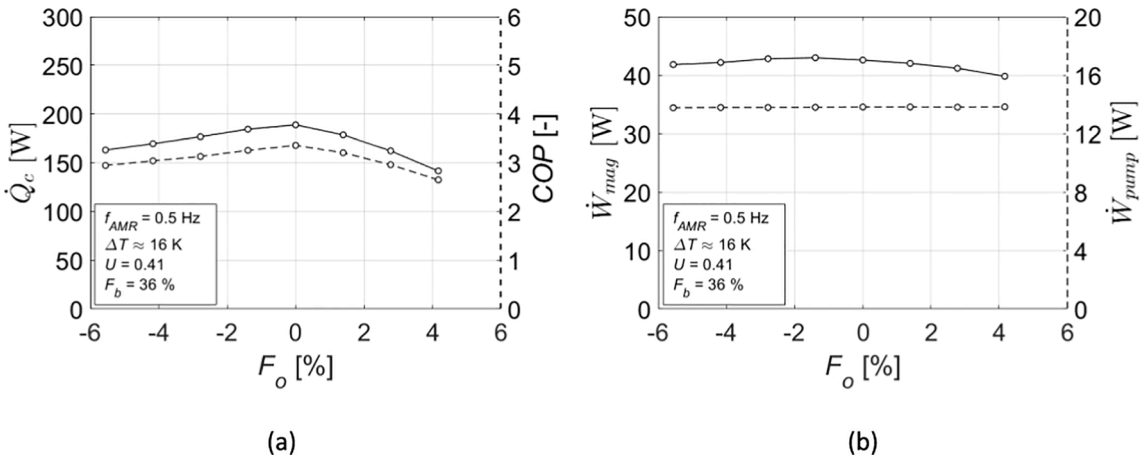

Fig. 6. (a) Cooling power (solid line) and COP (dashed line) vs the offset fraction. (b) Magnetic power (solid line) and pumping power (dashed line) vs the offset fraction.

cold and hot reservoir temperatures were about 285 K and 301 K, respectively, hence, keeping the temperature span fixed within some variation. The results indicate that $\dot{Q}_c$ reaches a maximum of 189 W, at an optimum offset fraction, which corresponds to the centered case. When the magnetic field and fluid flow profiles are centered, the solid refrigerant executes an AMR cycle similar to the Brayton-like AMR cycle. The heat transfer between the MCM and the heat transfer fluid during the cold and hot blows will then become more efficient, and a higher amount of heat can be exchanged in a blow period, resulting in a higher maximum specific cooling power [59]. The *COP* is also highest when the magnetic field and flow profiles are centered. When the offset fraction is changed, the cooling power reduces faster while the system input power remains relatively constant, resulting in a negative effect on the *COP*.

Shifting the offset fraction and thus the fluid flow from the optimum to earlier/later in the AMR cycle reduces the cooling performance by up to 25 %, probably due to higher (irreversible) heat transfer losses when the profiles are not centered. This highlights the importance of synchronizing the flow profile with the magnetic field profile in question. Positive offset fractions, i.e., when the fluid blow periods begin later in the AMR cycle than the center case, result in a greater performance reduction, whereas, negative offset fractions cause less of a performance reduction. This finding is consistent with previous modeling work [39]. Our results also share some similarities with a recent study by Griffith et al. [28], but only for tests run for small blow fractions. According to the authors, the optimal delay time varies with the blow fraction, and moving the center of the two profiles closer to the ends can enhance the cooling capacity for larger blow fractions. This cannot be verified in the present study, as the effect of the delay time on the device performance was only evaluated for a constant blow fraction.

Fig. 6b indicates that the timing has only a small impact on the AMR device's power consumption, which concurs with the findings in Ref. [28]. The pumping power is unaffected by changing the offset fraction, however, the magnetic power transferred into the regenerators is somewhat higher when the offset fraction is closer to the optimum value. Aligning the midpoint of the magnetic field and flow profiles leads to an AMR cycle closer to the Brayton cycle, which requires the highest magnetic power input compared to the shifted profiles [59]. However, the variation in the magnetic power between the centered and shifted cases is no more than 7 %. In general, once the optimum offset fraction has been determined, it should be a fixed parameter throughout the AMR device testing at different operating conditions. Therefore, all following experiments are conducted with an optimum offset fraction of 0 %, i.e., the perfect synchronization between magnetic field and fluid flow ($\tau_d = 0$).

3.3. Pressure drop and system power consumption

Fig. 7 shows the pressure drop data as a function of the fluid blow fraction for three utilizations and two temperature spans. In the following experiments, the cycle frequency was fixed at 1.4 Hz. For a given utilization, the pressure drop increased with lowering the blow period, and hence with increasing the no-flow period. As a result, the flow is almost completely obstructed and the pressure drop increases, which is caused by the larger cycle average mass flow rate required to realize the same utilization [28,33,34]. Higher utilization factors cause a rise in the pressure drop owing to a higher volume flow rate pumped through the AMR, as previously shown [58]. The large pressure drop of packed bed AMRs will confine any efficiency optimization, particularly at low fluid blow fractions. Thin parallel plates [60,61] and microchannels [62] are alternative regenerator geometries with decreased flow resistance that can provide better system efficiency at higher utilizations.

The behavior of the system power consumption as a function of the blow fraction is depicted in Fig. 9a and Fig. 9b. For all experiments the offset, τ_d, is 0, which was found to give best performance. The pumping power increases as the average blow fraction decreases and utilization increases, resulting from the larger volume flow rate and system pressure drop. This observation was also made in earlier studies [31–33]. It also seems that the utilization has less of an effect on the pumping power at larger blow fractions, as the difference in the pumping power between

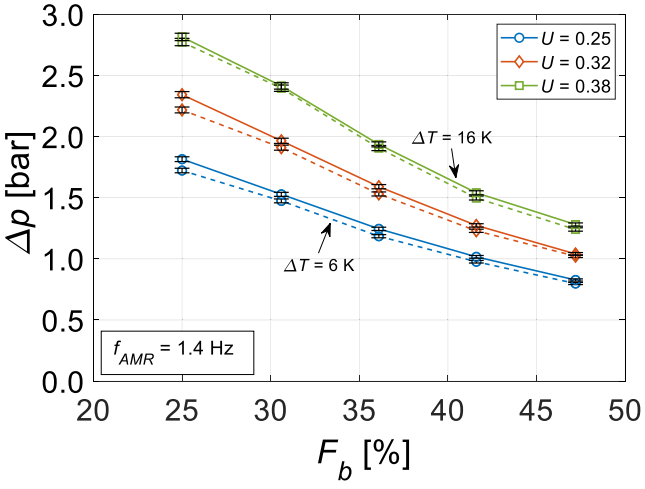

Fig. 7. Pressure drop as a function of blow fraction for different utilizations at low temperature span (dashed lines) and high temperature span (solid lines).

the lowest and highest utilization factor decreases with increasing blow fraction. In terms of the magnetic power demand, it is roughly maximum for the lowest blow fraction of 30.6 %, and this trend is consistent for both temperature spans. Blow fractions slightly above that value do not show large changes in the magnetic power. With increasing blow periods, however, the magnetic power decreases considerably. This was also demonstrated in Refs. [31,32], while another study found no apparent trend with regard to the blow fraction [33]. In addition, the magnetic power increases with utilization because of a greater degree of overlapping of the internal thermodynamic cycles between neighboring particles of the MCM within the AMR [59]. Nakashima et al. [33] made a similar observation based on the measurements of the mechanical torque.

Furthermore, the reservoir temperature span has only a small effect on the pumping power, despite the fact that there are some temperature-dependent changes in the viscosity of the heat transfer fluid at the regenerator cold end, as reported previously [22,42]. The magnetic power, on the other hand, is more sensitive to the temperature span. This is because of both the larger thermodynamic work required to transport heat over a larger span (cf. Eq. (11)) and the increased magnetic force between the AMRs and the magnet circuit [51]. The AMRs become more ferromagnetic as the cold reservoir temperature decreases, which, for this magnet design causes increased axial loading on the magnet bearings and couplings and therefore increased friction losses.

3.4. Cooling power and second-law efficiency

In a magnetic refrigerator, high cooling capacities at a high efficiency are desired. The effect of varying the blow fractions on the AMR cooling capacity is shown in Fig. 9a. The experimental data used to generate the plots were the same as previously described. The cooling power increases up to a blow fraction of 41.6 %, and a higher blow fraction presents no further improvement in the cooling power. The sharp drop in the cooling capacity when increasing the blow fraction from 41.6 to 47.1 % may be explained by a reduced convective heat transfer, on the one hand, causing an increased heat loss through the AMR. The heat transfer duration, on the other hand, may be longer than the maximum heat transfer needed, resulting in some overcooling during the cold blow or some overheating during the hot blow, which obliterate the temperature gradient. A blow fraction of 41.6 % in the AMR cycle seems to be optimal in terms of the cooling capacity, and it is independent of the reservoir temperature span.

Reduced blow periods (and longer no-flow periods) result in lower cooling capacities and second-law efficiencies. When the blow fractions are reduced, the cold and hot blows are concentrated in the periods when the magnetic field intensity is highest and lowest, respectively [33,34]. Lower blow fractions also imply that the cold and hot blows are performed over a shorter period of time, increasing the amplitude of the average mass flow rate (or superficial velocity). This decreases the Number of Transfer Units (NTU) [34], but increases the total entropy generation, resulting in thermal losses occurring inside the AMR. Three sources contribute to the increase in the entropy generation: viscous dissipation caused by internal fluid friction through the packed bed, (poor) interstitial heat transfer (or larger temperature differences) between solid and fluid phases, and larger (solid and fluid) axial heat conduction through the AMR [63]. From an AMR perspective, these sources of irreversibilities should be minimized for an optimum AMR performance. Thus, smaller blow fractions reduce the regenerator thermal effectiveness and hence the AMR cooling performance.

Similar investigations on the effect of the blow fraction on the AMR cooling capacity yielded contradictory results [32–34]. The authors found that lowering the blow fraction, regardless of the temperature span, leads to higher cooling capacities. These observations, however, were made with a rectified sinusoidal waveform of the magnetic field [32,33] or a sinusoidal field waveform [34]. For a field waveform with a near step change, which is similar to the present work, Nakashima et al. [32] showed in their simulation that reducing the blow fraction had no effect on the cooling capacity.

The behavior of the second-law efficiency as a function of the blow fraction is shown in Fig. 9b. The general trend is that the lowest blow fraction of 25 % leads to the lowest efficiencies, which is owing to the increased power consumption associated with shorter blow periods (see Fig. 8). At a higher temperature span, the efficiency follows the same trend as the cooling power, which increased up to a blow fraction of 41.6 %. The second-law efficiency was then calculated to be about 17.4 % for a utilization of 0.32, which is greater than the efficiency previously reported for the AMR device under similar operating conditions but with a blow fraction of 36.1 % [43]. This demonstrates the possibility for a greater thermodynamic efficiency when higher blow fractions are used. It should be noted that the behavior of the *COP* as a function of the blow fraction and utilization is similar to that of the second-law efficiency for a given temperature span. For comparison, the vapor compression system from Chung and Choi [47] gave a second-law efficiency of 22.9 % over a temperature span of 13 K.

At a lower span, however, the efficiency increases linearly with the blow fraction, and maximum efficiencies are calculated for the highest blow fraction of 47.2 %. The difference in the efficiency at different temperature spans may be explained by considering the contribution of the cooling capacity to the *COP*. When the blow fraction is increased from 41.6 to 47.2 %, the cooling capacity drops more significantly at a higher temperature span. On average, the cooling power decreases by up to 52 % at a higher span, but only by 23 %, when the span is reduced. Further improvements in the second-law efficiency can be made with decreasing utilization, as lower volume flow rates reduce the pressure drop across the regenerators.

The cooling performance maps (second-law efficiency vs cooling power) reveal useful operating points for the AMR device at a high temperature span of 16 K (Fig. 9c) and a low span of 6 K (Fig. 9d), respectively. At lower span, the cooling capacity follows a near linear trend with the utilization (Fig. 9d). The cooling capacity can be enhanced by increasing the utilization, but this is at the cost of a reduced efficiency due to a larger pumping power and magnetic power input. Hence, at the lowest utilization, the AMR provides the lowest cooling capacities at minimum losses. At higher span, on the other hand, no linear trend between the utilization and cooling capacity was observed (Fig. 9d), and highest values of the utilization result in a reduced cooling capacity. For most blow fractions, the lowest utilization results in the highest cooling capacity and second-law efficiency at a high temperature span. From a thermodynamic perspective, operating the AMR with a blow fraction of 41.6 % is the most efficient, as the AMR can achieve high cooling capacities at a high system efficiency.

3.5. Temperature pulldown

The temperatures of the working fluid exiting the cold and hot heat exchangers during the pulldown test are shown in Fig. 10a for average blow fractions of 30.6, 36.1, and 41.6 %. The AMR device was run at a frequency of 1.4 Hz and a flow rate of about 1300 L/h ($U = 0.36$). The cold and hot reservoir temperatures were set to around 287 K and 301 K, respectively. The reservoir set points only become relevant as the reservoir temperature begins to approach the set temperature. During startup, the working fluid on the cold and hot reservoir begins to pulldown from near room temperature (about 295 K). When the device and the external heat exchangers are turned on, the cold fluid reservoir temperature quickly cools down, while the hot fluid reservoir temperature steadily increases. The cold and hot heat exchanger set temperatures were reached after around 1500 s. It can be seen that the tests performed at shorter blow periods (and longer no-flow periods) favor a faster temperature pulldown, which is related to the fact that these conditions also exhibit the highest steady state cooling power. There is also a clear trend that lowering the blow fraction leads to a faster establishment of the given temperature span, which is about 14 K

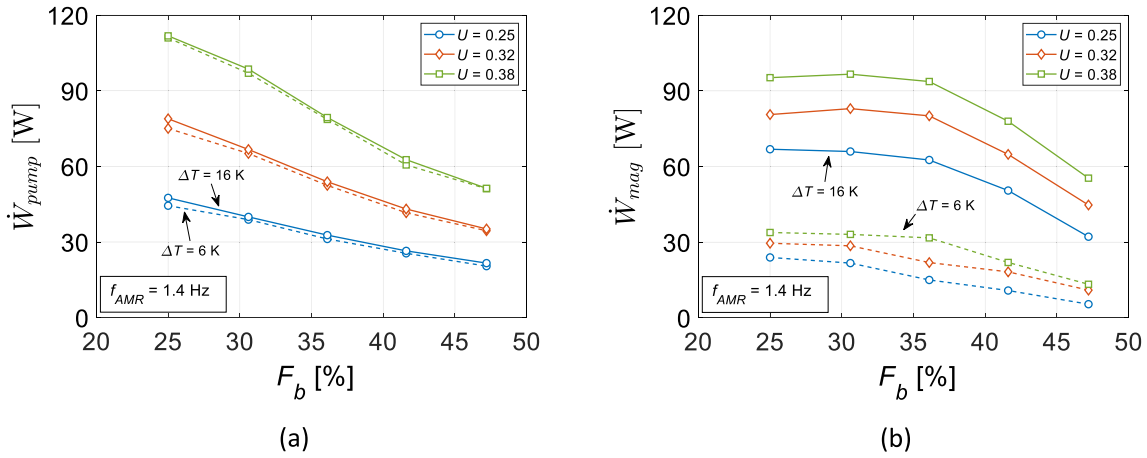

Fig. 8. (a) Pumping power as a function of blow fraction for different utilizations at low temperature span (dashed lines) and high temperature span (solid lines). (b) Magnetic power as a function of blow fraction for different utilizations at low temperature span (dashed lines) and high temperature span (solid lines).

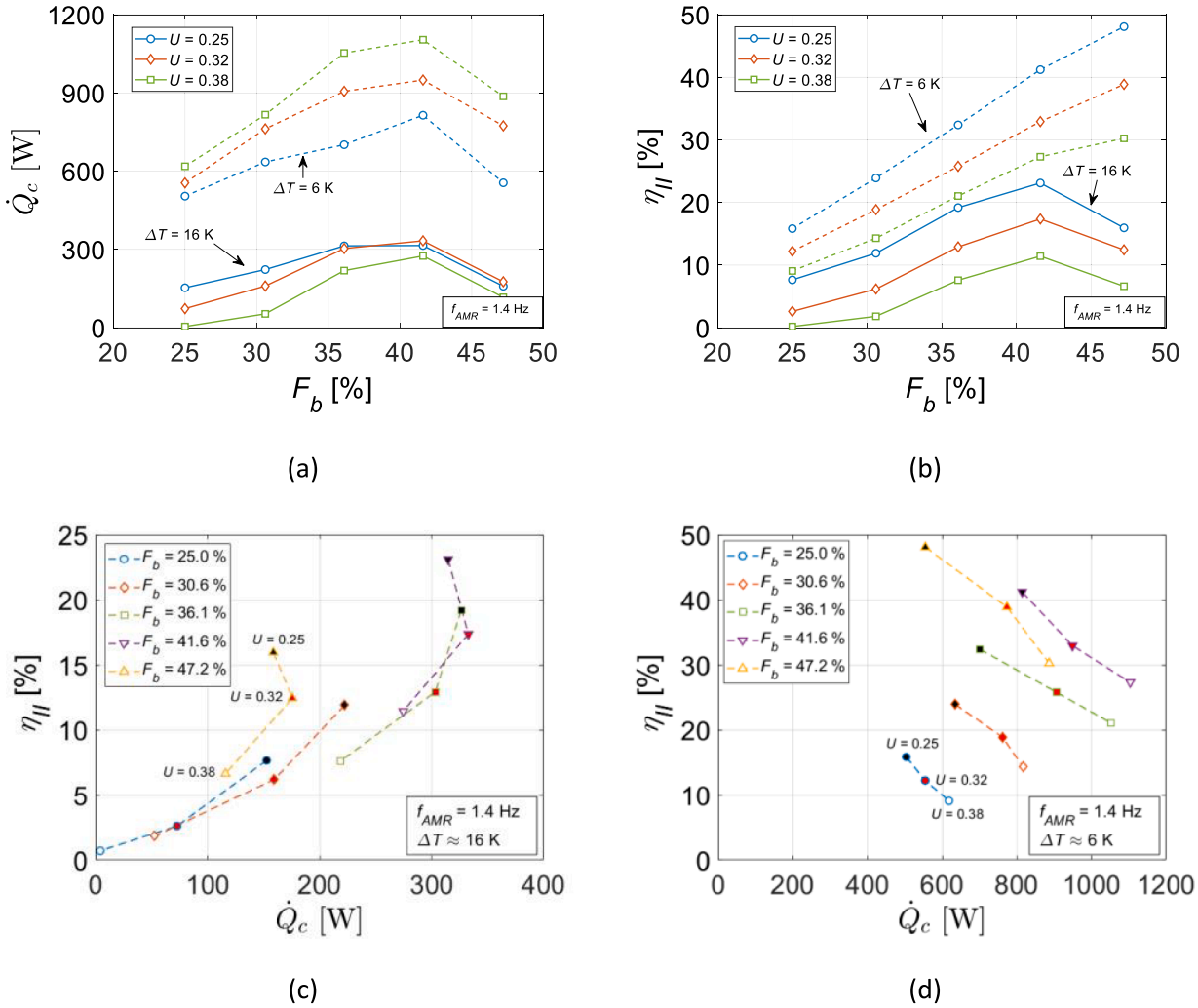

Fig. 9. (a) Cooling power as a function of blow fraction for different utilizations at low temperature span (dashed lines) and high temperature span (solid lines). (b) Second-law efficiency as a function of blow fraction for different utilizations at low temperature span (dashed lines) and high temperature span (solid lines). (c) Cooling performance maps (second-law efficiency vs cooling power) for different blow fractions and utilizations. (d) Cooling performance maps (second-law efficiency vs cooling power) for different blow fractions and utilizations.

(Fig. 10b). Reducing the blow fraction concentrates the cold and hot blows in the period where the magnetic field intensity is highest and lowest, respectively [31,33], and this increases the average magnetic field change during the flow period [33,34]. As a result, a smaller blow fraction seems to be beneficial in terms of attaining a quicker temperature pulldown. In particular, the rotary AMR system is about 30 %

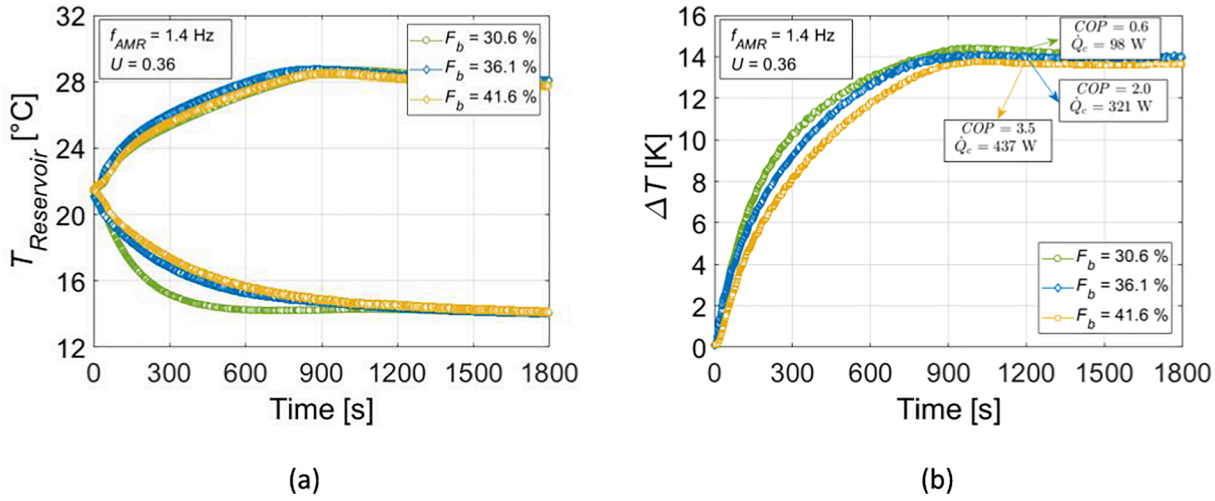

Fig. 10. (a) Cold and hot reservoir temperatures vs time at different blow fractions, (b) Reservoir temperature spans vs time at different blow fractions. The performance metrics stated in the textbox were obtained after reaching steady-state operating conditions.

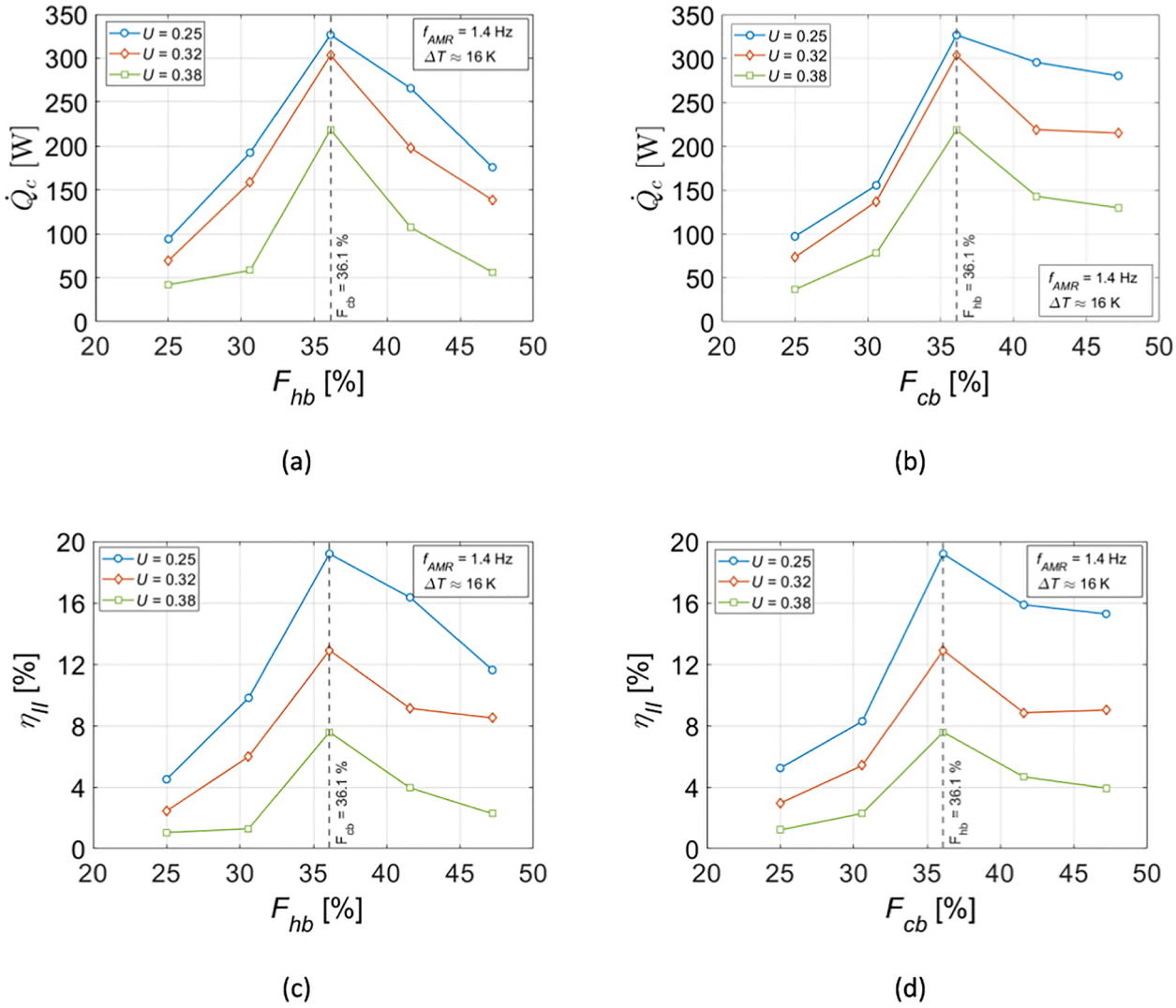

Fig. 11. (a) Cooling power as a function of varying hot blow fractions for different utilizations, while keeping the cold blow fraction constant at 36.1 %. (b) Cooling power as a function of varying cold blow fractions for different utilizations, while keeping the hot blow fraction constant at 36.1 %. (c) Second-law efficiency as a function of varying hot blow fractions for different utilizations, while keeping the cold blow fraction constant at 36.1 %. (d) Second-law efficiency as a function of varying cold blow fractions for different utilizations, while keeping the hot blow fraction constant at 36.1 %.

quicker in achieving an approximately 14 K temperature span when the blow fraction is lowered from 41.6 to 30.6 %. However, the shorter blow periods result in a reduced efficiency and cooling capacity once steady state is achieved, as indicated in Fig. 10b. Hence, after a steady-state temperature span is reached, a different valve operating mode may be considered that increases the fluid blow fractions and hence the AMR cooling performance. It can thus be concluded that the optimum blow fraction (30.6 %) to achieve a quick temperature pulldown is different from the optimum blow fraction (41.6 %) to maximize the cooling capacity and AMR efficiency.

3.6. Blow fraction differences between the cold and hot blows

In the ideal AMR cycle, the cold and hot blow periods are usually identical. However, as stated earlier, variations in the flow resistance in the two blow directions may cause disparities between the two blows in actual AMR devices. In MagQueen, this can be investigated by varying the value of the blow fraction difference between the cold and hot blows. If, for example, the LPVs open for a shorter (longer) period than the HPVs throughout the cycle, the cold blow period will be shorter (longer) than the hot blow period. Similarly, if the HPVs open for a shorter (longer) period than the LPVs, the hot blow period will be shorter (longer) than the cold blow period. During the operation of MagQueen, these different valve opening scenarios may occur. The effect of blow fraction differences between the cold and hot fluid blows on the cooling capacity and AMR efficiency is summarized in Fig. 11.

Fig. 11a and Fig. 11b show that non-identical cold and hot blow periods lead to significant reductions in the cooling capacity, and this trend is similar for different utilization factors. With an increase in the blow fraction difference between the LPVs and HPVs, the cooling capacity decreases dramatically. The reduction in the cooling capacity is even more pronounced for cold and hot blow periods that are shorter than the reverse blow period. At a utilization of 0.25, for instance, when the hot blow period is slightly shorter or longer than the cold blow, the cooling capacity drops by 41 % and 19 %, respectively. Similarly, the second-law efficiency is highest when the cold and hot blow fractions are identical and then decreases continuously with an increase in the blow fraction differences between the LPVs and HPVs (Fig. 11c and Fig. 11d). At a utilization of 0.25, for instance, when the hot blow period is slightly shorter or longer than the cold blow, the second-law efficiency drops by 49 % and 15 %, respectively. The results of the performance metrics hence indicate a greater imbalance in the AMR heat transfer effectiveness for blows that are shorter than the reverse blow.

4. Conclusion

The fluid flow characteristics of the parallel hydraulic circuit of a rotary multi-bed magnetic refrigeration system were investigated. The flow control mechanism comprised electrically actuated high-pressure and low-pressure solenoid valves responsible for the cold and hot blows, respectively. Flow resistance measurements were found to be useful to determine flow imbalances during the two blow periods and between individual regenerator beds. The refrigerator operated best when the magnetic field and fluid flow profiles were centered, and shifting the flow profile did not improve the cooling performance. Varying the cold and hot blow fractions between 25 and 47 % enables the control of the refrigerator performance metrics during operation. When the fluid blow fractions were reduced, the cooling capacity and refrigerator efficiency decreased due to a reduced regenerator thermal effectiveness during longer no-flow periods. Analysis of the system power consumption revealed that shorter blow fractions (or waveforms) cause both a higher pumping power due to an increased fluid pressure drop and a higher magnetic power. With the two temperature spans studied, the best blow fraction was about 41.6 %. At that blow fraction, a maximum cooling capacity of about 1100 W was obtained when operating the device at 1.4 Hz, a utilization of 0.38, and a reservoir temperature span of 6 K, which corresponds to a second-law efficiency of 27.3 %. It was also demonstrated that reducing the blow fractions can be suitable for applications that require a fast pulldown, but this is at the expense of a lower device efficiency at steady state. Hence, depending on the type of application for the magnetocaloric system, the solenoid valves may be operated in either a time-saving mode (i.e., lower blow fraction) to achieve a quick temperature pulldown or an energy-saving mode (i.e., higher blow fraction) to maximize the device efficiency. Future research will examine the potential of realizing partial load conditions to achieve higher system efficiencies.

Declaration of Competing Interest

The authors declare that they have no known competing financial interests or personal relationships that could have appeared to influence the work reported in this paper.

Data availability

Data will be made available on request.

Acknowledgements

This work was in part financed by the RES4Build project, which received funding from the European Union's Horizon 2020 research and innovation program under grant agreement No. 814865.

References

[1] J. He, J. Wu, H. Zhang, Y. Zhang, B. Lu, Numerical simulation of a fully solid-state micro-unit regeneration magnetic refrigerator with micro Peltier elements, Appl. Therm. Eng. 186 (2021), 116545, https://doi.org/10.1016/j.applthermaleng.2021.116545.
[2] A. Cavallini, Working fluids for mechanical refrigeration - Invited paper presented at the 19th International Congress of Refrigeration, The Hague, Int. J. Refrig. 19 (1996) (August 1995) 485–496, https://doi.org/10.1016/S0140-7007(96)00008-4.
[3] V. Franco, J.S. Blázquez, B. Ingale, A. Conde, The Magnetocaloric Effect and Magnetic Refrigeration Near Room Temperature: Materials and Models, Annu. Rev. Mater. Res. 42 (2012) 305–342, https://doi.org/10.1146/annurev-matsci-062910-100356.
[4] J. Tušek, A. Kitanovski, U. Tomc, C. Favero, A. Poredoš, Experimental comparison of multi-layered La-Fe-Co-Si and single-layered Gd active magnetic regenerators for use in a room-temperature magnetic refrigerator, Int. J. Refrig. 37 (2014) 117–126, https://doi.org/10.1016/j.ijrefrig.2013.09.003.
[5] U. Legait, F. Guillou, A. Kedous-Lebouc, V. Hardy, M. Almanza, An experimental comparison of four magnetocaloric regenerators using three different materials, Int. J. Refrig. 37 (2014) 147–155, https://doi.org/10.1016/j.ijrefrig.2013.07.006.
[6] L.M. Maier, P. Corhan, A. Barcza, H.A. Vieyra, C. Vogel, J.D. Koenig, O. Schäfer-Welsen, J. Wöllenstein, K. Bartholomé, Active magnetocaloric heat pipes provide enhanced specific power of caloric refrigeration, Commun. Phys. 3 (2020) 186, https://doi.org/10.1038/s42005-020-00450-x.
[7] A. Tura, A. Rowe, Permanent magnet magnetic refrigerator design and experimental characterization, Int. J. Refrig. 34 (2010) 628–639, https://doi.org/10.1016/j.ijrefrig.2010.12.009.
[8] D.S. Arnold, A. Tura, A. Ruebsaat-Trott, A. Rowe, Design improvements of a permanent magnet active magnetic refrigerator, Int. J. Refrig. 37 (2014) 99–105, https://doi.org/10.1016/j.ijrefrig.2013.09.024.
[9] P.V. Trevizoli, A.T. Nakashima, J.R. Barbosa Jr., Performance evaluation of an active magnetic regenerator for cooling applications – part II: Mathematical modeling and thermal losses, Int. J. Refrig. 72 (2016) 206–217, https://doi.org/10.1016/j.ijrefrig.2016.07.010.
[10] A. Maiorino, M.G. Del Duca, U. Tomc, J. Tušek, A. Kitanovski, C. Aprea, A numerical modelling of a multi-layer LaFeCoSi Active magnetic regenerator by using Artificial Neural Networks, Appl. Therm. Eng. 197 (2021), https://doi.org/10.1016/j.applthermaleng.2021.117375.
[11] M.A. Richard, A.M. Rowe, R. Chahine, Magnetic refrigeration: Single and multimaterial active magnetic regenerator experiments, J. Appl. Phys. 95 (2004) 2146–2150, https://doi.org/10.1063/1.1643200.
[12] S. Jacobs, J. Auringer, A. Boeder, J. Chell, L. Komorowski, J. Leonard, S. Russek, C. Zimm, The performance of a large-scale rotary magnetic refrigerator, Int. J. Refrig. 37 (2013) 84–91, https://doi.org/10.1016/j.ijrefrig.2013.09.025.
[13] J.A. Lozano, M.S. Capovilla, P.V. Trevizoli, K. Engelbrecht, C.R.H. Bahl, J. R. Barbosa Jr., Development of a novel rotary magnetic refrigerator, Int. J. Refrig. 68 (2016) 187–197, https://doi.org/10.1016/j.ijrefrig.2016.04.005.
[14] D. Eriksen, K. Engelbrecht, C.R.H. Bahl, R. Bjørk, K.K. Nielsen, A.R. Insinga, N. Pryds, Design and experimental tests of a rotary active magnetic regenerator

prototype, Int. J. Refrig. 58 (2015) 14–21, https://doi.org/10.1016/j.ijrefrig.2015.05.004.
[15] C. Aprea, A. Greco, A. Maiorino, C. Masselli, The energy performances of a rotary permanent magnet magnetic refrigerator, Int. J. Refrig. 61 (2016) 1–11, https://doi.org/10.1016/j.ijrefrig.2015.09.005.
[16] Z. Cheng, H. Jiaohong, Y. Hongwei, J. Peiyu, C. Juan, L. Cuilan, L. Zhaojie, Z. Yingde, Design and research of the room temperature magnetic wine cabinet, in: Refrig. Sci. Technol., 2016: pp. 63–66. https://doi.org/10.18462/iir.thermag.2016.0090.
[17] T. Okamura, N. Hirano, Improvement of the Performance of Room Temperature Magnetic Refrigerator using Gd-alloy, J. Japan Soc. Appl. Electromagn. Mech. 21 (2013) 10–14, https://doi.org/10.14243/jsaem.21.10.
[18] L. Yuan, S. Qian, J. Yu, Numerical study on the multi-layered magnetocaloric regenerators, Appl. Therm. Eng. 204 (2022), 118001, https://doi.org/10.1016/j.applthermaleng.2021.118001.
[19] S. Lionte, A. Barcza, M. Hittinger, M. Risser, C. Muller, M. Katter, Recent experimental results of first order LaFeSi-based magnetocaloric materials in an Active Magnetic Regeneration device, in: Refrig. Sci. Technol., 2018: pp. 56–61. https://doi.org/10.18462/iir.thermag.2018.0008.
[20] B. Monfared, B. Palm, New magnetic refrigeration prototype with application in household and professional refrigerators, in: Refrig. Sci. Technol., 2016: pp. 146–149. https://doi.org/10.18462/iir.thermag.2016.0142.
[21] S. Dall'Olio, M. Masche, J. Liang, A.R. Insinga, D. Eriksen, R. Bjørk, K.K. Nielsen, A. Barcza, H.A. Vieyra, N. v. Beek, H.N. Bez, K. Engelbrecht, C.R.H. Bahl, Novel design of a high efficiency multi-bed active magnetic regenerator heat pump, Int. J. Refrig. 132 (2021) 243–254. https://doi.org/10.1016/j.ijrefrig.2021.09.007.
[22] K. Engelbrecht, D. Eriksen, C.R.H. Bahl, R. Bjørk, J. Geyti, J.A. Lozano, K. K. Nielsen, F. Saxild, A. Smith, N. Pryds, Experimental results for a novel rotary active magnetic regenerator, Int. J. Refrig. 5 (2012) 3–10, https://doi.org/10.1016/j.ijrefrig.2012.05.003.
[23] C.R.H. Bahl, K. Engelbrecht, D. Eriksen, J.A. Lozano, R. Bjørk, J. Geyti, K. K. Nielsen, A. Smith, N. Pryds, Development and experimental results from a 1 kW prototype AMR, Int. J. Refrig. 37 (2013) 78–83, https://doi.org/10.1016/j.ijrefrig.2013.09.001.
[24] M.A. Benedict, S.A. Sherif, D.G. Beers, M.G. Schroeder, Design and performance of a novel magnetocaloric heat pump, Sci. Technol. Built Environ. 22 (2016) 520–526, https://doi.org/10.1080/23744731.2016.1185889.
[25] B. Huang, J.W. Lai, D.C. Zeng, Z.G. Zheng, B. Harrison, A. Oort, N.H. van Dijk, E. Brück, Development of an experimental rotary magnetic refrigerator prototype, Int. J. Refrig. 104 (2019) 42–50, https://doi.org/10.1016/j.ijrefrig.2019.04.029.
[26] J.A. Lozano, K. Engelbrecht, C.R.H. Bahl, K.K. Nielsen, D. Eriksen, U.L. Olsen, J. R. Barbosa Jr., A. Smith, A.T. Prata, N. Pryds, Performance analysis of a rotary active magnetic refrigerator, Appl. Energy. 111 (2013) 669–680, https://doi.org/10.1016/j.apenergy.2013.05.039.
[27] R. Bjørk, C.R.H. Bahl, K.K. Nielsen, The lifetime cost of a magnetic refrigerator, Int. J. Refrig. 63 (2016) 48–62, https://doi.org/10.1016/j.ijrefrig.2015.08.022.
[28] L. Griffith, A. Czernuszewicz, J. Slaughter, V. Pecharsky, Active magnetic regenerative cooling with smaller magnets, Int. J. Refrig. 125 (2021) 44–51, https://doi.org/10.1016/j.ijrefrig.2021.01.018.
[29] R. Bjørk, K. Engelbrecht, The influence of the magnetic field on the performance of an active magnetic regenerator (AMR), Int. J. Refrig. 34 (2010) 192–203, https://doi.org/10.1016/j.ijrefrig.2010.07.004.
[30] U. Plaznik, J. Tušek, A. Kitanovski, A. Poredoš, Numerical and experimental analyses of different magnetic thermodynamic cycles with an active magnetic regenerator, Appl. Therm. Eng. 59 (2013) 52–59, https://doi.org/10.1016/j.applthermaleng.2013.05.019.
[31] F.P. Fortkamp, D. Eriksen, K. Engelbrecht, C.R.H. Bahl, J.A. Lozano, J. R. Barbosa Jr., Experimental investigation of different fluid flow profiles in a rotary multi-bed active magnetic regenerator device, Int. J. Refrig. 91 (2018) 46–54, https://doi.org/10.1016/j.ijrefrig.2018.04.019.
[32] A.T.D. Nakashima, S.L. Dutra, P.V. Trevizoli, J.R. Barbosa Jr., Influence of the flow rate waveform and mass imbalance on the performance of active magnetic regenerators. Part II: Numerical simulation, Int. J. Refrig. 93 (2018) 159–168, https://doi.org/10.1016/j.ijrefrig.2018.07.005.
[33] A.T.D. Nakashima, S.L. Dutra, P.V. Trevizoli, J.R. Barbosa Jr., Influence of the flow rate waveform and mass imbalance on the performance of active magnetic regenerators. Part I: Experimental analysis, Int. J. Refrig. 93 (2018) 236–248, https://doi.org/10.1016/j.ijrefrig.2018.07.004.
[34] R. Teyber, P.V. Trevizoli, I. Niknia, T.V. Christiaanse, P. Govindappa, A. Rowe, Experimental performance investigation of an active magnetic regenerator subject to different fluid flow waveforms, Int. J. Refrig. 74 (2017) 38–46, https://doi.org/10.1016/j.ijrefrig.2016.10.001.
[35] Z. Li, K. Li, X. Guo, X. Gao, W. Dai, M. Gong, J. Shen, Influence of timing between magnetic field and fluid flow in a rotary magnetic refrigerator, Appl. Therm. Eng. 187 (2021), https://doi.org/10.1016/j.applthermaleng.2020.116477.
[36] D. Eriksen, K. Engelbrecht, C.R.H. Bahl, R. Bjørk, K.K. Nielsen, Effects of flow balancing on active magnetic regenerator performance, Appl. Therm. Eng. 103 (2016) 1–8, https://doi.org/10.1016/j.applthermaleng.2016.03.001.
[37] A.T.D. Nakashima, S.L. Dutra, J.R. Barbosa Jr., Experimental Evaluation of the Flow Imbalance in an Active Magnetic Experimental, 9th World Conf, Exp. Heat Transf. Fluid Mech, Thermodyn, 2017.
[38] J. Holladay, R. Teyber, K. Meinhardt, E. Polikarpov, E. Thomsen, C. Archipley, J. Cui, J. Barclay, Investigation of bypass fluid flow in an active magnetic regenerative liquefier, Cryogenics (Guildf). 93 (2018) 34–40, https://doi.org/10.1016/j.cryogenics.2018.05.010.
[39] D. Eriksen, K. Engelbrecht, C.R.H. Bahl, R. Bjørk, K.K. Nielsen, A.R. Insinga, S. Dall'Olio, N. Pryds, Experimental studies with an active magnetic regenerating refrigerator, Refrig. Sci. Technol. (2015) 926–933. https://doi.org/10.18462/iir.icr.2015.0812.
[40] P.V. Trevizoli, M.S. Capovilla, G.F. Peixer, A.T. Nakashima, J.A. Lozano, J. R. Barbosa Jr., Influence of void volume and inlet flow maldistribution on the performance of thermal regenerators, Refrig. Sci. Technol. (2016) 83–86, https://doi.org/10.18462/iir.thermag.2016.0102.
[41] Y. You, S. Yu, Y. Tian, X. Luo, S. Huang, A numerical study on the unsteady heat transfer in active regenerator with multi-layer refrigerants of rotary magnetic refrigerator near room temperature, Int. J. Refrig. 65 (2016) 238–249, https://doi.org/10.1016/j.ijrefrig.2016.02.002.
[42] M. Masche, J. Liang, S. Dall'Olio, K. Engelbrecht, C.R.H. Bahl, Performance analysis of a high-efficiency multi-bed active magnetic regenerator device, Appl. Therm. Eng. 199 (2021) 117569. https://doi.org/10.1016/j.applthermaleng.2021.117569.
[43] M. Masche, J. Liang, K. Engelbrecht, C.R.H. Bahl, Performance assessment of a rotary active magnetic regenerator prototype using gadolinium, Appl. Therm. Eng. 204 (2022), 117947, https://doi.org/10.1016/j.applthermaleng.2021.117947.
[44] C. Aprea, A. Greco, A. Maiorino, An application of the artificial neural network to optimise the energy performances of a magnetic refrigerator, Int. J. Refrig. 82 (2017) 238–251, https://doi.org/10.1016/j.ijrefrig.2017.06.015.
[45] S. Qian, L. Yuan, J. Yu, G. Yan, Variable load control strategy for room-temperature magnetocaloric cooling applications, Energy. 153 (2018) 763–775, https://doi.org/10.1016/j.energy.2018.04.104.
[46] S. Qian, L. Yuan, J. Yu, An online optimum control method for magnetic cooling systems under variable load operation, Int. J. Refrig. 97 (2019) 97–107, https://doi.org/10.1016/j.ijrefrig.2018.09.033.
[47] J.T. Chung, J.M. Choi, Design and performance study of the ground-coupled heat pump system with an operating parameter, Renew. Energy. 42 (2012) 118–124, https://doi.org/10.1016/j.renene.2011.08.054.
[48] P.V. Trevizoli, J.R. Barbosa Jr., A. Tura, D. Arnold, A. Rowe, Modeling of thermomagnetic phenomena in active magnetocaloric regenerators, J. Therm. Sci. Eng. Appl. 6 (2014), https://doi.org/10.1115/1.4026814.
[49] B.P. Vieira, H.N. Bez, M. Kuepferling, M.A. Rosa, D. Schafer, C.C. Plá Cid, H. A. Vieyra, V. Basso, J.A. Lozano, J.R. Barbosa Jr., Magnetocaloric properties of spheroidal La(Fe, Mn, Si)13Hy granules and their performance in epoxy-bonded active magnetic regenerators, Appl. Therm. Eng. 183 (2021), 116185, https://doi.org/10.1016/j.applthermaleng.2020.116185.
[50] Engineering equation solver, F-Chart Software V10 (2020) 889.
[51] P.V. Trevizoli, A.T. Nakashima, G.F. Peixer, J.R. Barbosa Jr., Performance evaluation of an active magnetic regenerator for cooling applications – part I : Experimental analysis and thermodynamic performance, Int. J. Refrig. 72 (2016) 192–205, https://doi.org/10.1016/j.ijrefrig.2016.07.009.
[52] H.W. Coleman, W.G. Steele, Experimentation, Validation, and Uncertainty Analysis for Engineers, John Wiley & Sons, 2018.
[53] J.L. Cadena, Designing a rotary magnetic refrigerator, Federal University of Santa Catarina, 2015, (2015).. PhD thesis.
[54] P.M. de Oliveira, On Air-Water Two-Phase Flows in Return Bends, Federal University of Santa Catarina, 2013, p. 155. Master's thesis.
[55] S. Ergun, Fluid Flow through Packed Column, Chem. Eng. Prog. 48 (1952) 89–94.
[56] A. Jourak, V. Frishfelds, J.G.I. Hellström, T.S. Lundström, I. Herrmann, A. Hedström, Longitudinal Dispersion Coefficient: Effects of Particle-Size Distribution, Transp. Porous Media. 99 (2013) 1–16, https://doi.org/10.1007/s11242-013-0159-5.
[57] Z.C. Chang, P.H. Chen, Flow channeling effect on a regenerator's thermal performance, Cryogenics (Guildf). 38 (1998) 191–196, https://doi.org/10.1016/S0011-2275(97)00133-1.
[58] P.V. Trevizoli, Y. Liu, A. Tura, A. Rowe, J.R. Barbosa Jr., Experimental assessment of the thermal-hydraulic performance of packed-sphere oscillating-flow regenerators using water, Exp. Therm. Fluid Sci. 57 (2014) 324–334, https://doi.org/10.1016/j.expthermflusci.2014.06.001.
[59] A. Kitanovski, J. Tušek, U. Tomc, U. Plaznik, M. Ožbolt, A. Poredoš, Magnetocaloric Energy Conversion: From Theory to Applications, Springer, 2015.
[60] C.R.H. Bahl, K. Navickaitė, H. Neves Bez, T. Lei, K. Engelbrecht, R. Bjørk, K. Li, Z. Li, J. Shen, W. Dai, J. Jia, Y. Wu, Y. Long, F. Hu, B. Shen, Operational test of bonded magnetocaloric plates, Int. J. Refrig. 76 (2017) 245–251, https://doi.org/10.1016/j.ijrefrig.2017.02.016.
[61] J. Tušek, A. Kitanovski, A. Poredoš, Geometrical optimization of packed-bed and parallel-plate active magnetic regenerators, Int. J. Refrig. 36 (2013) 1456–1464, https://doi.org/10.1016/j.ijrefrig.2013.04.001.
[62] J. Liang, K. Engelbrecht, K.K. Nielsen, K. Loewe, H. Vieyra, A. Barcza, C.R.H. Bahl, Performance assessment of a triangular microchannel active magnetic regenerator, Appl. Therm. Eng. 186 (2021), 116519, https://doi.org/10.1016/j.applthermaleng.2020.116519.
[63] P.V. Trevizoli, D.P. Alcalde, J.R. Barbosa Jr., Entropy generation minimization analysis of passive and active magnetocaloric regenerators, Proc. 15th Int. Heat Transf. Conf. IHTC (2014. (2014).), https://doi.org/10.1615/ihtc15.hex.009007.